Ubiquitin-driven protein condensation promotes clathrin-mediated endocytosis

Feng Yuan[1], Sadhana Gollapudi[1], Kasey J. Day[1], Grant Ashby[1], Arjun Sangani[1], Brandon T. Malady[1], Liping Wang[2], Eileen M. Lafer[2], Jon M. Huibregtse[3], Jeanne C. Stachowiak[1,4]*

[1] Department of Biomedical Engineering, The University of Texas at Austin, Austin, TX, United States.
[2] Department of Biochemistry and Structural Biology, The University of Texas Health Science Center at San Antonio, San Antonio, TX, United States.
[3] Department of Molecular Biosciences, The University of Texas at Austin, Austin, TX, United States.
[4] McKetta Department of Chemical Engineering, The University of Texas at Austin, Austin, TX, United States.
**To whom correspondence should be addressed: jcstach@austin.utexas.edu*

Abstract

Clathrin-mediated endocytosis is an essential cellular pathway that enables signaling and recycling of transmembrane proteins and lipids. During endocytosis, dozens of cytosolic proteins come together at the plasma membrane, assembling into a highly interconnected network that drives endocytic vesicle biogenesis. Recently, multiple labs have reported that early endocytic proteins form liquid-like condensates, which provide a flexible platform for the efficient assembly of endocytic vesicles. Given the importance of this network in the dynamics of endocytosis, how might cells regulate its stability? Many receptors and endocytic proteins are ubiquitylated, while early endocytic proteins such as Eps15 contain ubiquitin-interacting motifs. Therefore, we examined the influence of ubiquitin on the stability of the early endocytic protein network. In vitro, we found that recruitment of small amounts of polyubiquitin dramatically increased the stability of Eps15 condensates, suggesting that ubiquitylation could nucleate endocytic sites. In live cell imaging experiments, a version of Eps15 that lacked the ubiquitin-interacting motif failed to rescue defects in endocytic initiation created by Eps15 knockout. Furthermore, fusion of Eps15 to a deubiquitinase enzyme destabilized nascent endocytic sites within minutes. These results suggest that ubiquitylation drives assembly of the flexible protein network responsible for catalyzing endocytic events. More broadly, this work illustrates a biophysical mechanism by which ubiquitylated transmembrane proteins at the plasma membrane could regulate the efficiency of endocytic recycling.

Introduction

Endocytosis, which is responsible for internalizing proteins and lipids from the plasma membrane, is essential for a myriad of cellular functions including signaling, nutrient import, and recycling[1]. Clathrin-mediated endocytosis is the best understood pathway of cellular internalization[2]. In the earliest moments of clathrin-mediated endocytosis, initiator proteins including Eps15, Fcho, and Intersectin assemble together to create a nascent endocytic site[2,3]. The resulting network of initiators recruits adaptor proteins, such as AP2, CALM/AP180, and Epsin, among many others, which in turn recruit clathrin triskelia[2,4]. Assembly of triskelia into an icosahedral lattice works in concert with adaptor proteins to induce membrane curvature and vesicle budding[2,4]. As clathrin coated structures grow, transmembrane cargo proteins are recruited into them. Many cargo proteins contain biochemical motifs that mediate binding to endocytic adaptor proteins[5], while post-translational modifications, such as ubiquitylation, drive uptake of transmembrane proteins destined for degradation or recycling[6–9]. Once the clathrin coat is fully assembled and loaded with cargo proteins, scission occurs, resulting in the formation of clathrin-coated vesicles that bud off from the plasma membrane, followed by uncoating[2,3].

Interestingly, the early initiator proteins of clathrin-mediated endocytosis are not incorporated into endocytic vesicles[10,11]. Instead, they function like catalysts, remaining at the plasma membrane to initiate multiple rounds of endocytosis. To promote growth of a clathrin-coated vesicle, the initiator network must remain flexible, allowing clathrin and its adaptors to accumulate and rearrange. Similarly, as the vesicle matures, the network of initiators must ultimately dissociate from it, allowing the final coated vesicle to depart into the cytosol. In line with these requirements, recent work has shown that initiator proteins, which contain substantial regions of intrinsic disorder, form liquid-like assemblies that undergo rapid exchange[12–15]. Specifically, Day and colleagues showed that Eps15 and Fcho1/2 form a liquid-like network, which exhibits optimal catalytic activity when its level of assembly is maintained within an intermediate range[12]. When the network assembly was too weak, the fraction of endocytic events that were short-lived, likely aborting without creating a vesicle, increased. Conversely, an excessively strong initiator network led to the accumulation of overly stable, stalled endocytic structures. Work by Wilfling and colleagues suggests that such structures may mature into autophagic sites, rather than resulting in endocytosis[13,14]. More broadly, Kozak and colleagues found that Ede1, the yeast homolog of Eps15, mediates assembly of liquid-like condensates that incorporate many endocytic components, suggesting that the requirement for a flexible network of endocytic initiator proteins may be broadly conserved[15].

Motivated by these findings, we set out to understand how cells regulate the stability of the early endocytic network. As noted above, Eps15/Ede1 is a key component of this

network. Interestingly, several studies have suggested that ubiquitylation can play an important role in mediating interactions between Eps15, cargo proteins, and endocytic adaptor proteins[9,16–19]. Specifically, Hicke and collaborators identified a ubiquitin association domain near the C terminus of Ede1, which enabled interactions between Ede1 and ubiquitinated proteins[9,16]. Similarly, Paolo di Fiore and colleagues reported that the two ubiquitin interacting motifs (UIMs) at the C terminus of Eps15 are essential for its interactions with ubiquitinated proteins[18]. Further, studies by Drubin and colleagues suggested that the ubiquitylation state of Ede1 plays an important role in endocytic dynamics in budding yeast[20].

These findings led us to ask whether ubiquitylation might impact the assembly of liquid-like networks of early endocytic proteins. Using purified proteins in vitro, we found that recruitment of small amounts of polyubiquitin significantly enhanced the stability of liquid-like Eps15 droplets, suggesting a potential role for ubiquitylation in nucleating endocytic sites. Through live cell imaging, we observed that expression of UIM-deficient Eps15 in cells lacking endogenous Eps15 failed to rescue the defect in clathrin-mediated endocytosis caused by Eps15 knockout. Similarly, removing ubiquitin from Eps15 and its close interactors by recruitment of an Eps15 variant containing a broad-spectrum deubiquitinase domain resulted in a significant destabilization of nascent endocytic sites. Finally, using an optogenetic approach, we found that this destabilization occurred within minutes following recruitment of deubiquitinases to endocytic sites. Collectively, these results suggest that ubiquitylation plays a critical role in stabilizing the flexible protein network responsible for catalyzing clathrin-mediated endocytosis.

Results

Polyubiquitin partitions strongly to liquid-like droplets of Eps15

We first asked to what extent monoubiquitin and polyubiquitin interact with liquid-like networks of Eps15. To address this question, we compared the partitioning of monoubiquitin (MonoUb) and lysine-63-linked tetra-ubiquitin (K63 TetraUb) into Eps15 droplets *in vitro*. Notably, K63-linked polyubiquitin chains are thought to play an important role in recycling of receptors from the cell surface[21–24]. Eps15 is composed of three major domains: the N-terminal region, which consists of three Eps15 Homology (EH) domains; a central coiled-coil domain, which is responsible for dimerization of Eps15; and an intrinsically disordered C-terminal domain[25]. The C-terminal domain contains a binding site for the α-subunit of the clathrin adaptor-protein complex AP2, two ubiquitin-interacting motifs (UIMs) (Figure 1a, top), and 15 tripeptide Asp-Pro-Phe (DPF) motifs[25–27]. The DPF motifs mediate oligomerization of Eps15 by binding to its N-terminal EH domains[25–27]. As previously reported, full-length Eps15 assembles into liquid-like droplets through these

multivalent interaction when added to a solution of 3% w/v PEG8000 in a buffer consisting of 20 mM Tris-HCl, 150 mM NaCl, 5 mM TCEP, 1 mM EDTA and 1 mM EGTA at pH 7.5[12] (Figure 1a, bottom, where ten percent of Eps15 molecules were labeled with the N-hydroxysuccinimide (NHS)-reactive dye, Atto 488 for visualization).

To examine the impact of ubiquitin of phase separation of Eps15, MonoUb and TetraUb, labeled with Atto 647, were added to Eps15 droplets at a final concentration of 1 μM and 0.25 μM, respectively, maintaining an equivalent mass per volume of ubiquitin. Images of the Eps15 droplets were collected after a 5-minute incubation. As shown in Figure 1b, c, both MonoUb and TetraUb partitioned uniformly into Eps15 droplets. However, the partition coefficient of TetraUb into Eps15 droplets, indicated by the ratio between the intensity of ubiquitin in the droplet (I_D) and the surrounding solution (I_S), was about twice that of MonoUb (4.1 ± 0.8 vs. 1.8 ± 0.2, Figure 1d), suggesting that Eps15 interacted more strongly with TetraUb, compared to MonoUb. Importantly, Eps15 droplets incubated with either MonoUb or TetraUb remained liquid-like, readily fusing and re-rounding upon contact (Figure 1e, f and Supplementary Information movie S1 and S2).

Further, MonoUb and TetraUb partitioned much more weakly into droplets consisting of a version of Eps15 that lacked its UIMs, Eps15ΔUIM (Δaa 851-896), (1.4 ± 0.1 and 1.5 ± 0.1 respectively, with no significant difference, Figure 1g, h and i). These results confirm that Eps15's UIMs play a key role in the partitioning of ubiquitin into Eps15 droplets, where both (i) Eps15-Eps15 interactions and (ii) Eps15-ubiquitin interactions are expected to exist within droplets (Figure 1j, k).

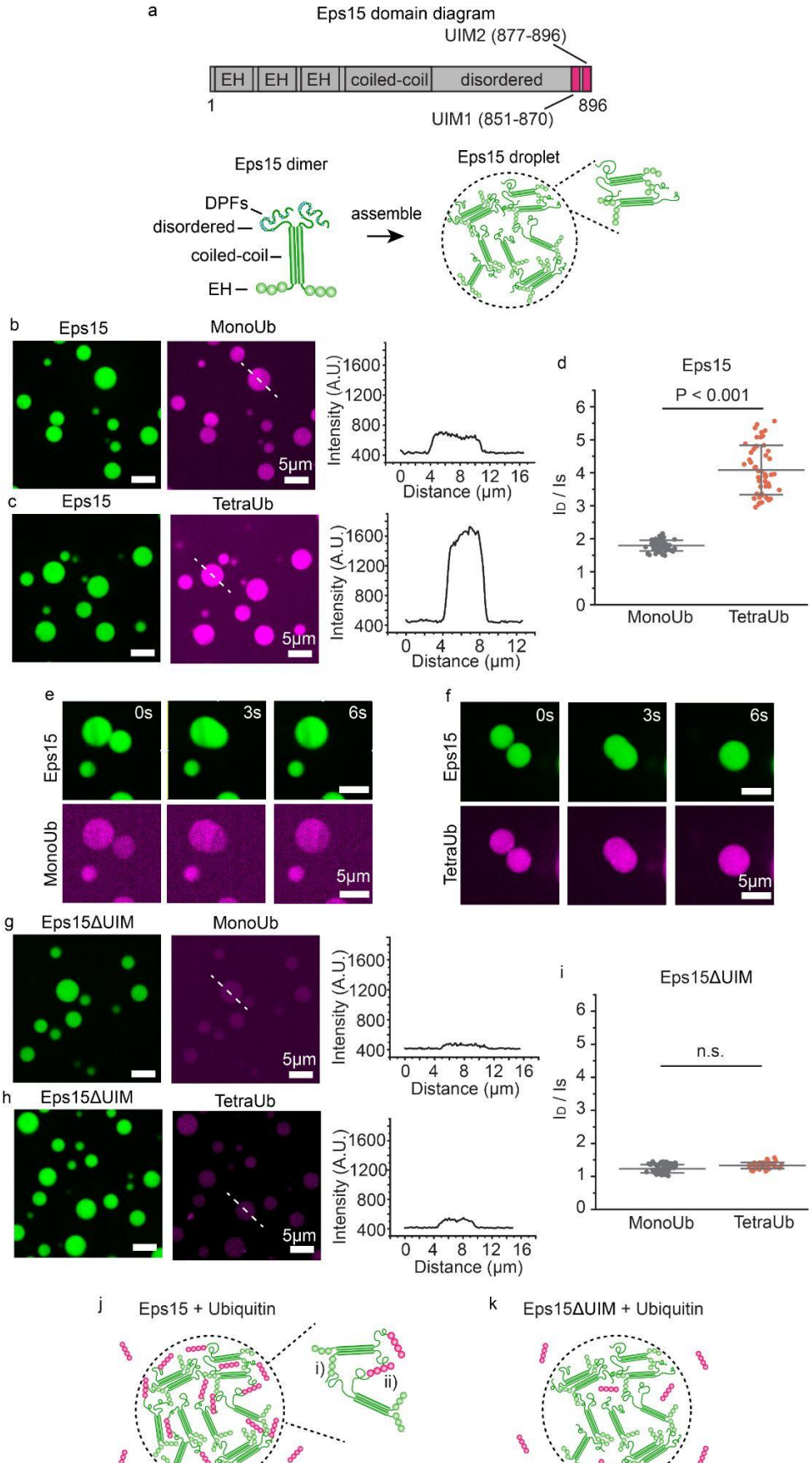
a
Eps15 domain diagram
UIM2 (877-896)
EH
EH
EH
coiled-coil
disordered
1
896
UIM1 (851-870)
Eps15 dimer
DPFs
disordered
coiled-coil
EH
assemble
Eps15 droplet
b
Eps15
MonoUb
5μm
Intensity (A.U.)
Distance (μm)
c
Eps15
TetraUb
5μm
d
Eps15
P < 0.001
ID / IS
MonoUb
TetraUb
e
0s
3s
6s
Eps15
MonoUb
5μm
f
0s
3s
6s
Eps15
TetraUb
5μm
g
Eps15ΔUIM
MonoUb
5μm
h
Eps15ΔUIM
TetraUb
5μm
i
Eps15ΔUIM
n.s.
MonoUb
TetraUb
j
Eps15 + Ubiquitin
i)
ii)
k
Eps15ΔUIM + Ubiquitin

Figure 1. Polyubiquitin partitions strongly into liquid-like droplets of Eps15. a, top: Schematic of Eps15 functional domains. Eps15 consists of three EH domains at its N terminus followed by a coiled-coil domain and a long disordered region containing two ubiquitin interacting motifs (UIMs) at the C terminal end. Bottom: cartoons depict domain organization of Eps15 in dimeric form. 15 tripeptide Asp-Pro-Phe (DPF) motifs are interspersed throughout the disordered region, which can bind the EH domains and allow itself to assemble into liquid-like droplets. **b, c,** Eps15 (7μM) droplets (green) incubated with 1μM MonoUb and 0.25μM K63 linkage TetraUb (magenta), respectively. Plots on the right depict intensity profile of ubiquitin channel along the white dashed line shown in the corresponding images. **d**, The distribution of the ubiquitin intensity ratio between the intensity inside the droplets (I_D) and the solution (I_S). In total 50 droplets were analyzed under each condition. **e, f**, Representative time course of fusion events between droplets containing Eps15 and MonoUb (**e**) and droplets containing Eps15 and TetraUb (f). **g-i**, Same with **b-d** except that droplets were formed with Eps15 mutant, Eps15ΔUIM, with the depletion of the two UIMs (aa 851-896). **j, k,** Pictorial representation of ubiquitin binding and partitioning into Eps15 droplets through interaction with UIMs at the C terminus of Eps15 (**j**) and deletion of UIMs impairs ubiquitin partitioning into Eps15 droplets (**k**). Inset in **j** shows the two types of interactions in Eps15-polyubiquitin network: i) DPF motif interacting with EH domain, and ii) polyubiquitin interacting with UIM domains. All droplet experiments were performed in 20 mM Tris-HCl, 150 mM NaCl, 5 mM TCEP, 1 mM EDTA and 1 mM EGTA at pH 7.5 with 3% w/v PEG8000. Error bars are standard deviation. Statistical significance was tested using an unpaired, two-tailed student's t test. All scale bars equal 5 μm.

Polyubiquitin promotes phase separation of Eps15 on membrane surfaces.

We next asked how the interaction between ubiquitin and Eps15 might impact assembly of Eps15 condensates on the surfaces of lipid membranes. To address this question, we purified Eps15 fused with an N-terminal 6 histidine tag (his-Eps15) and incubated it at a concentration of 0.5 μM with giant unilamellar vesicles (GUVs) consisting of 93 mol% POPC, 5 mol% DGS-NTA-Ni, and 2 mol% DP-EG10 biotin for coverslip tethering. Here, his-Eps15 was recruited to the surfaces of GUVs through binding between the histidine tag and Ni-NTA lipid headgroups (Figure 2a, left). His-Eps15 bound uniformly to the surfaces of GUVs (Figure 2a, left, and 2b), indicating that it alone does not phase separate on membrane surfaces, consistent with a previous report[12]. Similarly, when 0.5 μM his-Eps15 and 0.5 μM MonoUb were added simultaneously to GUVs, MonoUb was recruited to the membrane surface through its interaction with Eps15, and both proteins decorated the surfaces of GUVs uniformly (Figure 2c). However, when 0.5 μM his-Eps15 and 0.2 μM TetraUb were added simultaneously to GUVs, the two proteins co-partitioned into protein-rich (bright) and protein-depleted (dim) phases on GUV surfaces (Figure 2d and 2a, right), similar to previous observations of protein phase separation on GUVs[12,28]. Three-dimensional reconstruction of image stacks revealed that the bright regions formed hemispherical domains on GUVs, which were surrounded by dimmer regions, indicating phase separation (Figure S1), as quantified in Figure 2g. In contrast, when UIMs were removed from his-Eps15 (his-Eps15ΔUIM), neither MonoUb nor TetraUb could be strongly recruited to GUV surfaces, and his-Eps15ΔUIM bound uniformly to the

membrane surface, rather than phase separating (Figure 2e, f and g). These results illustrate that TetraUb promotes phase separation of Eps15 on membrane surfaces in a manner that depends upon Eps15's UIMs, suggesting that TetraUb strengthens the Eps15 network, likely by creating cross-links between Eps15 molecules (Figure 2a, right).

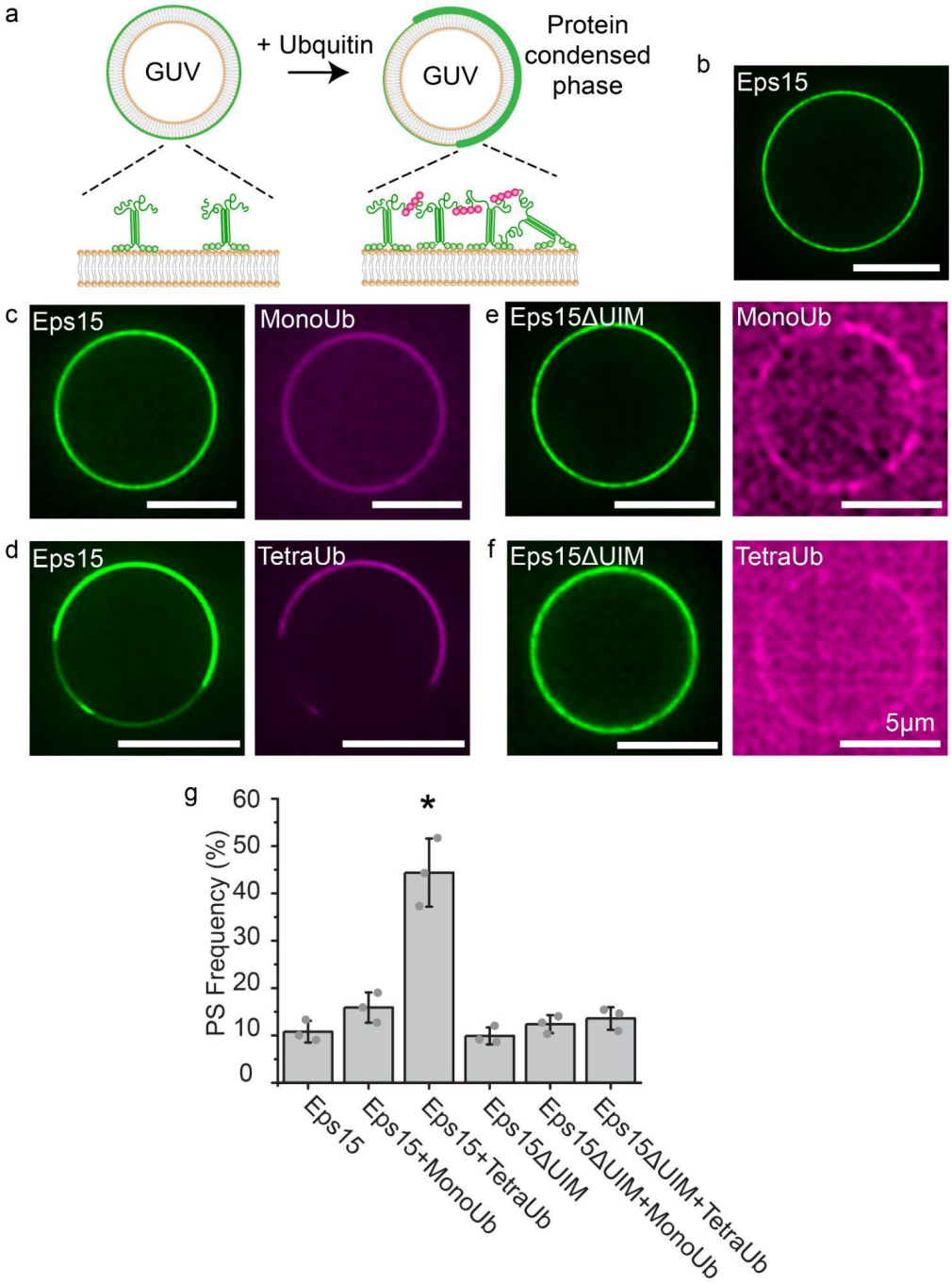

Figure 2. Polyubiquitin promotes phase separation of Eps15 on membrane surfaces. a, Cartoon depicting his-Eps15 binding to GUV membrane (left) and polyubiquitin driving Eps15 phase separation on

GUV membrane by linking Eps15 through interaction with the UIMs (right). **b-f**, Representative images of GUVs incubated with indicated proteins: 0.5 μM his-Eps15 alone (**b**), 0.5 μM his-Eps15 with 0.5 μM MonoUb (**c**), 0.5 μM his-Eps15 with 0.2 μM TetraUb (**d**), 0.5 μM his-Eps15ΔUIM with 0.5 μM MonoUb (**e**), and 0.5 μM his-Eps15ΔUIM with 0.2 μM TetraUb (**f**). All scale bars are 5 μm. **g**, Frequency of GUVs displaying protein-rich domains for each set of proteins. GUVs were counted as displaying protein-rich domains if they contained distinct regions in which protein signal intensity differed by at least two-fold and the bright region covered at least 10% of the GUV surface in any z-slice. For each bar, n = 3 biologically independent experiments (each individual dot) with at least 44 total GUVs for each condition. Data are mean ± SD. *: $P < 0.001$ compared to all other groups using unpaired, two-tailed student's t test. GUVs contain 93 mol% POPC, 5 mol% DGS-NTA-Ni, and 2 mol% DP-EG10-biotin. All experiments were conducted in 20 mM Tris-HCl, 150 mM NaCl, 5 mM TCEP at pH 7.5 buffer.

Eps15 knockout creates a significant defect in coated pit dynamics that cannot be rescued by a version of Eps15 that lacks the ubiquitin interacting motif.

Having demonstrated that polyubiquitin can promote phase separation of Eps15 *in vitro*, we next sought to evaluate the impact of interactions between Eps15 and ubiquitin during the dynamic growth and maturation of endocytic structures at the plasma membrane of living cells. Previous work has demonstrated that Eps15 plays an important role in stabilizing complexes of early endocytic proteins[29]. Importantly, the dynamic assembly of endocytic structures at the plasma membrane is a highly heterogeneous process. While most assemblies of endocytic proteins ultimately result in productive endocytic events, a minority of these assemblies have aberrant stability, resulting in their failure to develop into endocytic vesicles. In particular, endocytic assemblies that persist at the plasma membrane for less than 20 seconds are generally regarded as "short-lived" structures[30]. These unstable assemblies, which typically consist of a small number of proteins, often stochastically disassemble before forming a productive vesicle. Productive assemblies typically form vesicles and depart from the plasma membranes over timescales of 20 seconds to several minutes. In contrast, structures that persist at the plasma membrane for longer periods are typically characterized as "long-lived" structures[31]. These overly stable assemblies, which are often larger than productive endocytic structures, may fail to develop into endocytic vesicles.

While it is difficult to determine whether individual assemblies of endocytic proteins form productive vesicles, shifts in the lifetime of endocytic structures provide insight into the overall efficiency of endocytosis. Specifically, an increase in short-lived structures indicates a reduction in stability, while an increase in productive or long-lived structures indicates an increase in stability. Within this framework, Eps15 knockout has recently been shown to decrease the productivity of endocytosis by increasing the fraction of endocytic structures that are short-lived[12]. Building on this result, we assessed the impact of interactions between Eps15 and ubiquitin on the dynamics of endocytosis.

We evaluated endocytic dynamics in a human breast cancer-derived epithelial cell line, SUM159, which was gene edited to (i) knockout Eps15, and (ii) add a C-terminal halo-tag to the sigma2 subunit of AP2. As AP2 is the major adaptor protein of the clathrin-mediated endocytic pathway[32,33], the halo tag, bound to JF646 dye, was used to visualize and track endocytic structures in real-time during live cell imaging[34]. Imaging experiments were performed using total internal reflection fluorescence (TIRF) microscopy to isolate the plasma membrane of adherent cells. In TIRF images, endocytic structures appear as diffraction-limited fluorescent puncta in the JF646 channel, Figure 3a. Eps15, and its variants, described below, were tagged at their C-termini with mCherry for visualization, and appeared co-localized with puncta of AP2 (JF646), Figure 3a. Based on the literature cited above, we loosely classified endocytic structures that persisted at the plasma membrane for less than 20s as “short-lived”, structures that persisted from 20 - 180 seconds as “productive”, and structures that persisted for longer than 180 seconds as “long-lived”. Endocytic structures within each of these categories were observed in our experiments (Figure 3a) and the distribution of lifetimes for the full population of endocytic structures is shown in Figure 3b. In agreement with a recent report[12], Eps15KO cells had a significantly higher frequency of short-lived structures compared to wildtype cells with endogenous expression of Eps15 (15.4 ± 3.3% vs. 4.4 ± 1.3%, Figure 3b, c). This defect was effectively rescued by transient expression of wildtype Eps15 in Eps15KO cells (5.2 ± 1.6% vs. 4.4 ± 1.3% short-lived structures, Figure 3b, c).

We also analyzed the impact of Eps15 knockout on the intensity of endocytic structures in the AP2 channel, which, owing to the near 1:1 stochiometric ratio between AP2 and clathrin[35], serves as a proxy for the maturity and size of endocytic structures. This analysis revealed that Eps15 knockout resulted in significantly reduced AP2 intensity, suggesting less developed endocytic structures, compared to wildtype cells and knockout cells transiently expressing wildtype Eps15, Figure 3d and Figure S2. Specifically, histograms of AP2 intensity showed a shift towards smaller values when Eps15 was knocked out (850 ± 12, green dotted line, vs. 660 ± 5, red dotted line, in wildtype cells, Figure 3e), a defect which was rescued by transient expression of wildtype Eps15 in knockout cells (840 ± 9, black dotted line, vs. green dotted line, Figure 3e). Collectively, these results demonstrate that Eps15 knockout destabilizes endocytic structures, limiting their maturation.

Having established these controls, we next examined the impact of Eps15’s UIMs on its ability to promote efficient endocytosis. Specifically, we measured the extent to which a version of Eps15 lacking the UIMs (Eps15ΔUIM, as described above) could rescue the defect in endocytic dynamics created by knockout of the wildtype protein. Interestingly, we found that the elevated number of short-lived endocytic structures observed upon Eps15 knockout was not substantially reduced by expression of Eps15ΔUIM at equivalent levels to the level of Eps15wt required for full rescue, (15.1 ± 1.9% vs. 15.4 ± 3.3%, Figure

3b, c). Similarly, expression of Eps15ΔUIM failed to elevate the average AP2 intensity at endocytic sites significantly above levels measured in knockout cells (Figure 3d, no significant difference between Eps15ΔUIM and Eps15KO in AP2 intensity, and AP2 distribution peaked at 710 ± 9, black dotted line, vs. red dotted line, Figure 3e), indicating an inability to stabilize endocytic structures. These results suggest that Eps15's UIMs are essential to its ability to promote assembly and maturation of endocytic structures.

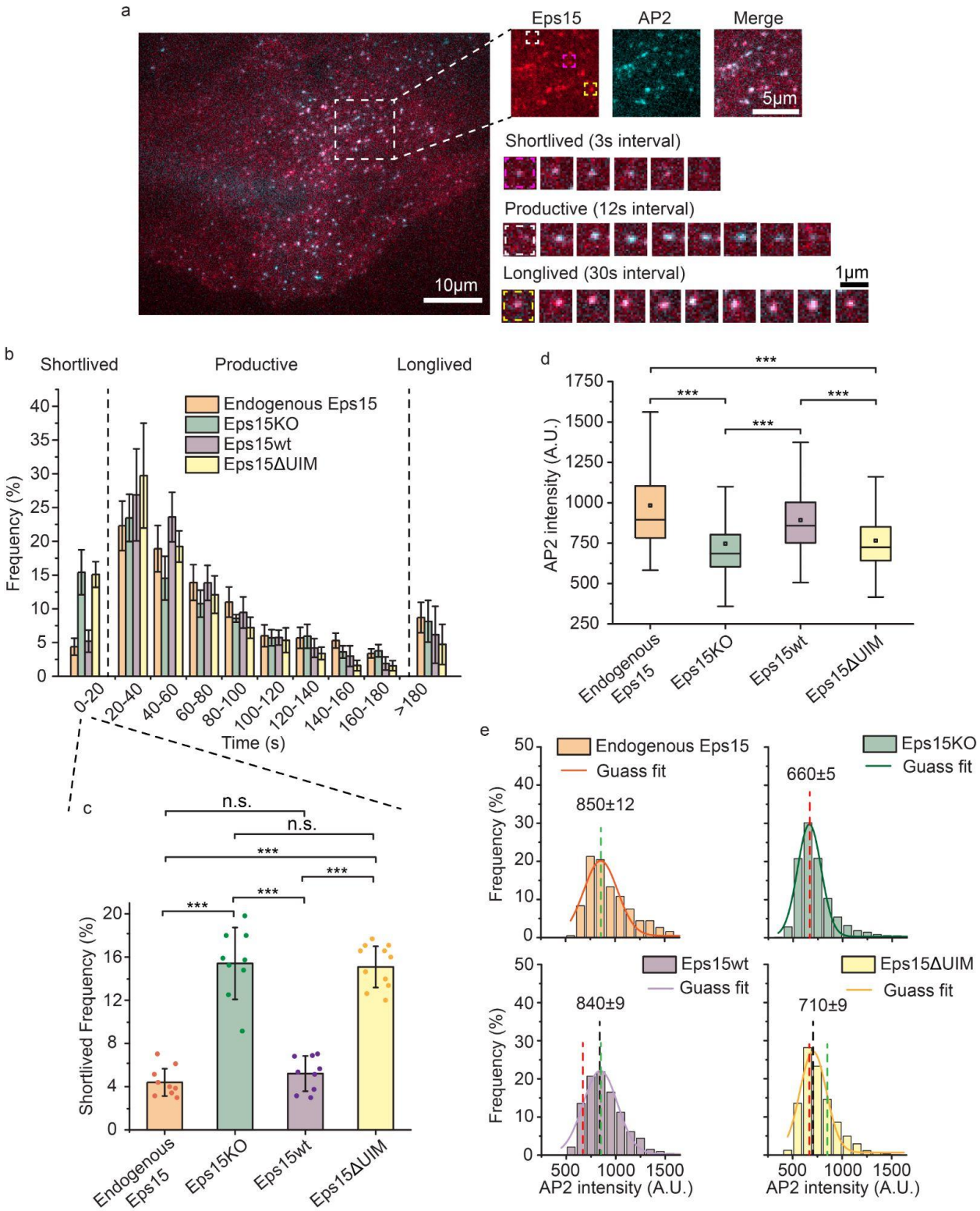

Figure 3. Eps15 knockout creates a significant defect in coated pit dynamics that cannot be rescued by a version of Eps15 that lacks the ubiquitin interacting motif. a, Representative image of a SUM cell expressing gene-edited AP-2 σ2-HaloTag: JF646 (cyan) and Eps15-mCherry (red). Large inset highlights

three representative clathrin-coated structures shown in smaller insets: short lived (pink), productive (white) and longlived (yellow) structures lasting 18 s, 96 s and > 5 min, respectively. Scale bars are labeled in the images. **b**, Histograms of lifetime distributions of clathrin-coated structures under different experimental groups. Endogenous Eps15 represents SUM cells that have endogenous Eps15 expression. Lifetime shorter than 20 s is considered short-lived, lifetime between 20 and 180 s is labeled as productive and structures lasted longer than 180 s are long-lived. Eps15KO represents SUM cells that were CRISPR modified to knockout alleles of endogenous Eps15. Eps15wt and Eps15ΔUIM represent Eps15KO cells transfected with wildtype Eps15 and Eps15 with the depletion of both UIM domains, respectively. mCherry was fused to the C terminus of Eps15 and Eps15ΔUIM for visualization. **c,** bar chat of the short-lived fraction for each group from **b,** error bars are standard deviation, dots represent the results from different samples. **d**, Box plot of endocytic pits AP2 intensity in all four groups. **e**, Histograms and the Guass fit of the AP2 intensity distribution tracked in endocytic pits under different experimental groups. Green dotted line indicates the peak distribution in Endogenous Eps15 cells, and red dotted line indicates the peak distribution in Eps15KO cells. For Endogenous Eps15 group, n = 9 biologically independent cell samples were collected and in total 2002 pits were analyzed. For Eps15KO, n = 9 and 2475 pits. Eps15wt, n = 9 and 2554 pits and Eps15ΔUIM, n = 11, 3952 pits. An unpaired, two-tailed student's t test was used for statistical significance. n.s. means no significant difference. ***: $P < 0.001$. All cell images were collected at 37°C.

Polyubiquitin elevates the melting temperature of liquid-like Eps15 networks.

The shorter lifetime of endocytic structures formed when Eps15ΔUIM replaces wild-type Eps15 suggests that loss of the UIMs destabilizes the network of early endocytic proteins. To test this idea, we sought to assess the impact of ubiquitin on the thermodynamic stability of liquid-like condensates of Eps15. For this purpose, we returned to the *in vitro* condensate system in Figure 1 and measured the temperature above which Eps15 condensates dissolve or melt, which is a key indicator of their stability[12]. Specifically, when we heated solutions of Eps15, liquid-like Eps15 droplets gradually dissolved, eventually melting such that the solution became homogenous (fully dissolved, Figure 4). The higher the melting temperature, the more energy is needed to prevent proteins from forming condensates, suggesting a more stable protein network.

To determine the melting temperature, images of Eps15 droplets were taken at each temperature as we heated the sample, starting from room temperature. As shown in Figure 4a, Eps15 droplets formed from a 7 μM protein solution, which gradually dissolved with increasing temperature and melted at approximately 32°C (Figure 4a), in agreement with a previous report[12]. We next examined the impact of ubiquitin on the melting temperature. Keeping Eps15 concentration at 7 μM, addition of 500 nM MonoUb slightly increased the melting temperature to 34°C (Figure 4b). In contrast, addition of 100 nM TetraUb raised the melting temperature more substantially from 32°C to 42°C (Figure 4c), suggesting that TetraUb is substantially more effective in stabilizing Eps15 condensates, in comparison to MonoUb. Using these data, we mapped a temperature-concentration phase diagram for Eps15 condensates (Figure 4d). Specifically, the relative fluorescence intensity of the droplets compared with the surrounding solution provided an estimate of

the relative protein concentration in the two phases, C_D and C_S, respectively. These concentrations represent the ends of a tie-line on a temperature-concentration phase diagram at each temperature. As the temperature increased, the intensity of the Eps15 droplets decreased (Figure 4a-c) and the tie-lines became shorter as C_D and C_S became more similar, Figure 4d. The two concentrations ultimately became equivalent above the melting temperature, owing to dissolution of the droplets, Figure 4d. These results are in line with a recent report showing that poly-ubiquitin can enhance phase separation of proteins involved in protein degradation and autophagy[36].

To assess the impact of Eps15's UIM domains, we mapped the phase diagram of Eps15ΔUIM droplets in the presence of either MonoUb or TetraUb (Figure 4f, g and Figure S3), keeping protein concentrations the same as those used in experiments with wild-type Eps15. The phase diagram indicated that neither MonoUb nor TetraUb had a significant impact on the melting temperature of condensates composed of Eps15ΔUIM, demonstrating that the stabilization effect observed with wildtype Eps15 arises from specific interactions between Eps15 and ubiquitin. Collectively, these results demonstrate that polyubiquitin not only partitions preferentially into Eps15 condensates (Figure 1) but can also help to crosslink and reinforce the protein network in a manner that is UIM-dependent (Figure 4e).

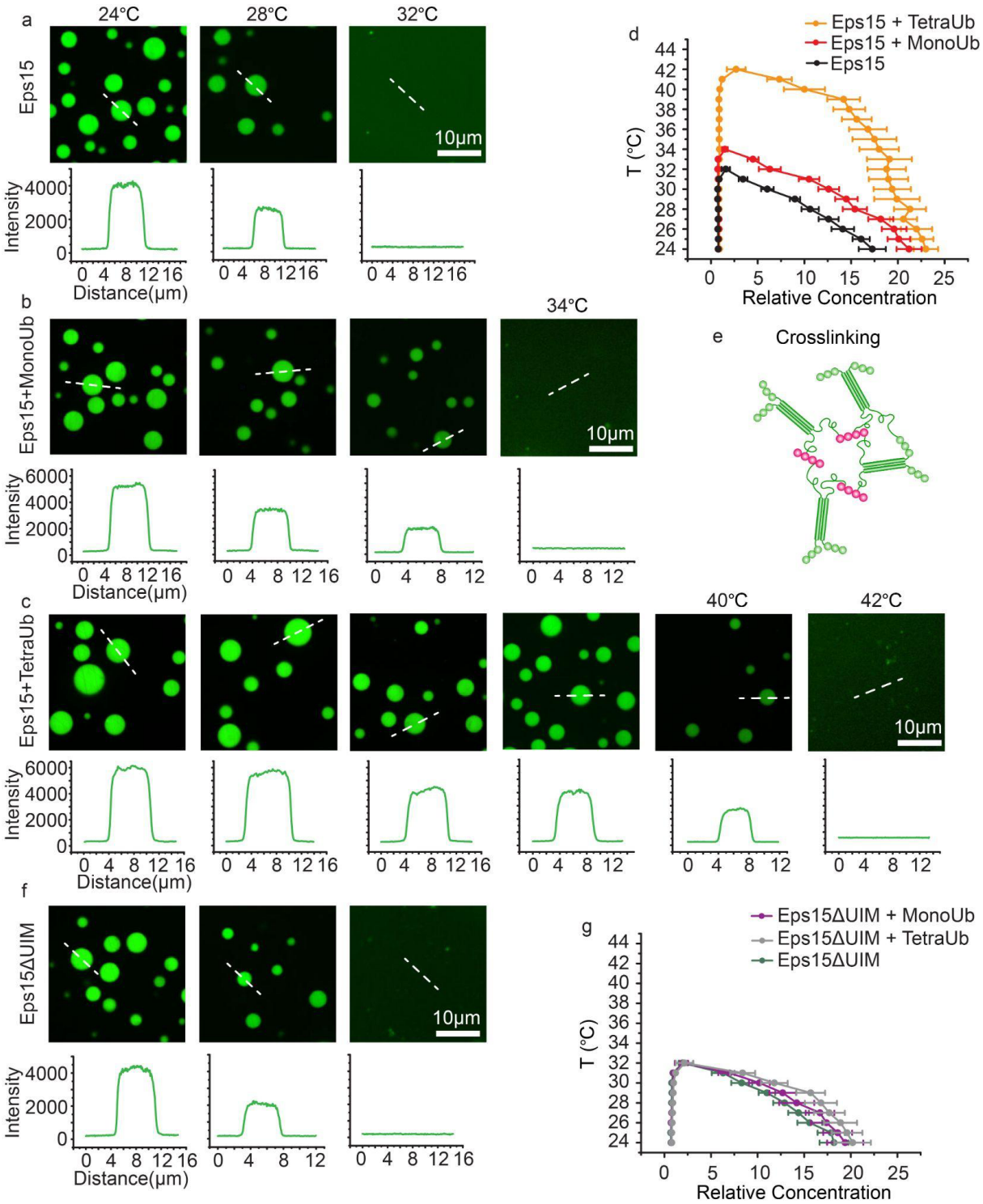

Figure 4. Polyubiquitin elevates the melting temperature of liquid-like Eps15 networks. a-c, f, Representative images of protein droplets at increasing temperatures. Plots show fluorescence intensity of Eps15 measured along dotted lines in each image. Droplets are formed from (**a**) 7 μM Eps15, (**b**) 0.5 μM MonoUb, 7 μM Eps15, (**c**) 0.1 μM TetraUb, 7 μM Eps15 and (**f**) 7 μM Eps15ΔUIM in 20 mM Tris-HCl, 150 mM NaCl, 5 mM TCEP, 1 mM EDTA and 1 mM EGTA at pH 7.5 buffer with 3% PEG8000. **d, g**, Phase diagram of Eps15/monoUb/TetraUb (**d**) and Eps15ΔUIM/MonoUb/TetraUb (**g**) droplets mapped by

Atto488-labelled Eps15/Eps15ΔUIM fluorescence intensity. Intensity was normalized based on the intensity of the solution. Dots on the right side are protein concentrations in droplets and dots on the left side are concentrations in solution. At least 20 droplets are analyzed under each temperature. Data are mean ± SD. Scale bars equal 10 μm. **e,** Schematic of polyubiquitin crosslinking and stablizing Eps15 network.

Fusion of a deubiquitinating enzyme to Eps15 results in about twice as many short-lived endocytic events than deletion of Eps15.

If polyubiquitin stabilizes endocytic protein networks, then stripping ubiquitin from the proteins that make up an endocytic site should disrupt the dynamics of endocytosis. To test this concept, we added a deubiquitinating enzyme (DUB) to Eps15 to remove ubiquitin modifications from Eps15 as well as its close interactors, which likely include other endocytic proteins and the intracellular domains of receptors that enter endocytic sites[37–39]. Using this approach, we sought to probe the broader sensitivity of endocytic assemblies to loss of ubiquitination. Here a "broad-spectrum" deubiquitinase, UL36, was adopted. UL36, which consists of the N-terminal domain (residues 15-260) of the type I Herpes virus VP1/2 tegument protein[37,40], cleaves both K63 and K48-linked polyubiquitin chains[38,40,41]. K63-linked chains are more traditionally associated with endocytic recycling[23,42], while K48-linked chains, which are mainly involved in targeting proteins for proteasomal degradation[42], have a less understood relationship with endocytosis. UL36 was inserted at the C-terminus of Eps15, prior to the mCherry tag, to create the fusion protein Eps15-DUB (Figure 5a). As a control for the potential non-specific impact of the DUB fusion on endocytic function, a catalytically inactive UL36, which contains a mutation of its core catalytic residues (Cys65 to Ala)[38,41], was inserted at the same position as the catalytically active UL36 to create the chimera, Eps15-DUB-dead (Figure 5a). We then expressed both Eps15-DUB and Eps15-DUB-dead in Eps15 knockout cells and tracked endocytic dynamics with TIRF microscopy, as described in Figure 3. TIRF images revealed clear colocalization of Eps15-DUB and Eps15-DUB-dead (mCherry) with endocytic sites, represented by fluorescent puncta in the AP2 (JF646) channel, Figure 5b. However, expression of Eps15-DUB in Eps15KO cells led to a further decrease in AP2 intensity (Figure 5b and Figure 5c, top, 570 ± 11) at endocytic sites compared to Eps15 knockout cells alone (Figure 5c, red dotted line), suggesting smaller, less mature endocytic sites. In contrast, expression of Eps15-DUB-dead restored AP2 intensity to a level more similar to wildtype cells (Figure 5b, and Figure 5c, bottom, 810 ± 12, vs. the green dotted line). Furthermore, the fraction of unstable, short-lived endocytic sites increased by more than 60% in cells expressing Eps15-DUB, compared to cells lacking Eps15 (27.5 ± 5.8% vs. 15.4 ± 3.3% Figure 5d). These results suggest that Eps15-DUB not only failed to rescue the defect caused by Eps15 knockout, but made the defect substantially larger, such that there is a strong bias toward unproductive, short-lived endocytic events when ubiquitin is removed from endocytic sites (Figure 5e). In contrast,

Eps15-DUB-dead provided a partial rescue of endocytic dynamics, reducing the fraction of short-lived structures to 10.7 ± 1.8%, Figure 5d. These results suggest that the importance of ubiquitylation to endocytosis likely extends beyond Eps15. In particular, if Eps15 were the only endocytic protein that relied on ubiquitin for its assembly, we would have expected Eps15-DUB to create no greater effect on endocytic dynamics than Eps15ΔUIM. These results could be explained by the presence of other UIMs within endocytic proteins, such as Epsin[18,16,43], which could interact with ubiquitin modifications on virtually any endocytic protein or transmembrane cargo protein.

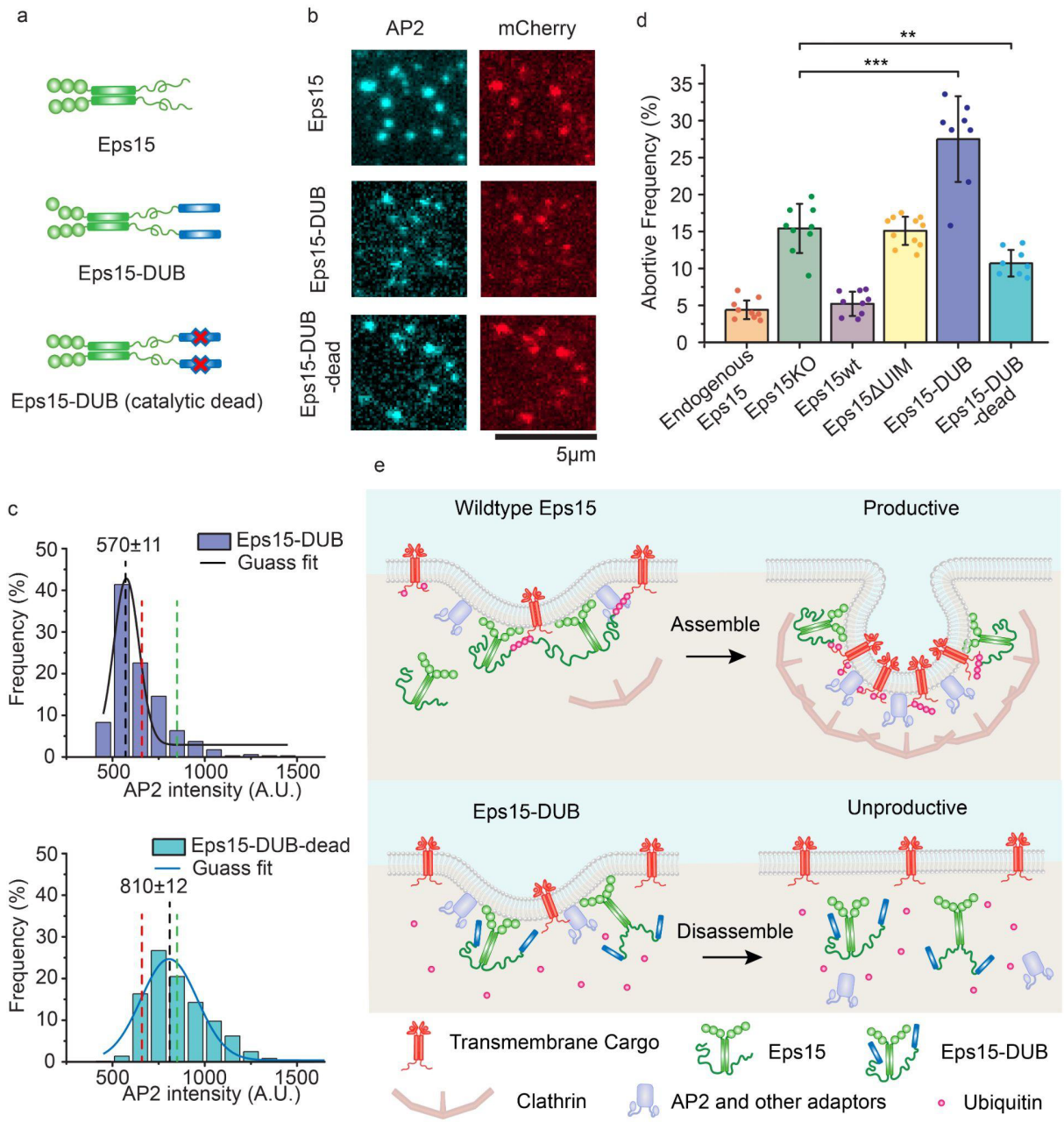

Figure 5. Fusion of a deubiquitinating enzyme to Eps15 results in even more short-lived endocytic events than deletion of Eps15. a, Schematic of Eps15 dimeric form, Eps15-DUB (deubiquitinase fused to C terminal end of Eps15), and Eps15-DUB-dead (same with DUB but with a mutation that makes DUB catalytically dead). mCherry is not shown in the cartoon but all three constructs have mCherry at their C terminus for visualization. **b**, Representative images showing Eps15, Eps15-DUB and Eps15-DUB-dead colocalization with AP2 in endocytic sites when Eps15KO SUM cells were transfected to express corresponding proteins. Scale bar = 5 μm. **c**, Histograms and the Guass fit of the AP2 intensity distribution tracked in endocytic pits when expressing Eps15-DUB (top) and Eps15-DUB-dead (bottom), respectively. The green dotted line and red dotted line are corresponding to Eps15KO group and endogenous Eps15 group in Figure 3. **d**, Frequency of short-lived structures under each condition. Endogenous Eps15, Eps15KO, Eps15wt and Eps15ΔUIM are adopted from the same data in shown in Figure 3. For Eps15-DUB, n = 8 biologically independent cell samples were collected and in total 1053 pits were analyzed. For Eps15-DUB-dead, n = 8 and 1464 pits were analyzed. Dots represent the frequency from each sample. An unpaired, two-tailed student's t test was used for statistical significance. **: $P < 0.01$, ***: $P < 0.001$. Error bars represent standard deviation. Cells were imaged at 37°C for all conditions. **e**, Schematic showing how polyubiquitin stabilizes the endocytic protein network by interacting with and cross-linking UIMs on endocytic proteins, resulting in productive clathrin-mediated endocytosis (Top). Removal of ubiquitin from the endocytic protein network using DUB decreases the network multivalency thus making the network less stable, resulting in less efficient clathrin-mediated endocytosis (bottom).

Light-activated recruitment of DUBs demonstrates that loss of ubiquitination destabilizes endocytic sites within minutes.

While the results in the previous section suggest the importance of ubiquitylation to endocytic dynamics, it is not clear whether the observed shifts result from an acute impact on endocytosis versus broader physiological changes resulting from expression of deubiquitinases. Therefore, we sought to develop a system that would allow us to measure endocytic dynamics immediately after recruitment of deubiquitinases to endocytic sites. For this purpose, we made use of our previous observation that monomeric Eps15, which is created by deletion of Eps15's coiled-coil domain, is not stably recruited to endocytic sites, likely owing to reduced affinity for the endocytic protein network[12]. Therefore, we created a chimeric protein in which Eps15's coiled-coil domain was replaced by a domain that forms dimers and oligomers upon blue light exposure, the photolyase homology region (PHR) of CRY2[44] (Figure 6a). As reported previously, the resulting chimera, Eps15-CRY2 assembles upon blue light exposure, resulting in its stable recruitment to endocytic sites[12].

Similarly, we found that when Eps15-CRY2 was transiently expressed in Eps15 knockout cells, it colocalized weakly with endocytic sites prior to blue light exposure (Figure 6b, top). The fraction of short-lived endocytic sites in these cells remained similar to the level in knockout cells (17.7 ± 4.4%, Figure 6h), consistent with previous findings that a monomeric version of Eps15 cannot rescue Eps15 knockout[12]. However, upon exposure to blue light, Eps15-CRY2 was recruited to endocytic sites (Figure 6b, bottom, and Figure

S4, fraction of pits showing Eps15 colocalization increased from 35.5 ± 5.5% to 74.1 ± 6%). Simultaneously with the increase in Eps15 recruitment, more AP2 was recruited to endocytic sites (mean AP2 intensity shifted from 740 ± 12 to 910 ± 16, Figure 6b, c, Supplementary Information Movie S3), suggesting increased stability and maturation of endocytic sites. Similarly, the fraction of short-lived endocytic structures was reduced to near wild type levels, 7.3 ± 3.2% (Figure 6h), confirming that light-induced assembly of Eps15 stabilized endocytic sites, rescuing the defects associated with Eps15 knockout[12]. Importantly, in these experiments, endocytic dynamics were consecutively measured before and after blue light exposure in each cell, such that changes associated with light-activated protein assembly were directly observed for individual cells (see Materials and Methods).

We next repeated these experiments in Eps15 knockout cells that transiently expressed a blue light activated Eps15 chimera fused to the UL36 deubiquitinase enzyme, Eps15-CRY2-DUB. Similar to Eps15-CRY2, in the absence of blue light, this protein colocalized weakly with endocytic sites (Figure 6d, top, Figure S4) and failed to substantially reduce the fraction of short-lived endocytic sites (16.5 ± 3.5%, Figure 6h). However, upon exposure to blue light, increased recruitment of this DUB-containing chimera to endocytic sites resulted in an 69% increase in the fraction of short-lived endocytic sites (27.9 ± 6.0%, Figure 6h), which correlated with a substantial reduction in recruitment of AP2 to endocytic sites (710 ± 8 to 550 ± 6, Figure 6e, Supplementary Information Movie S3). In contrast, expression of an Eps15-CRY2 chimera that contained the catalytically inactive DUB, Eps15-CRY2-DUB-dead, reduced the fraction of short-lived endocytic structures to near wild type levels (8.0 ± 3.0% vs. 7.3 ± 3.2%, Figure 6h) upon blue light exposure. Similarly, recruitment of AP2 to endocytic sites in cells expressing Eps15-CRY2-DUB-dead was similar to that in cells expressing Eps15-CRY2 (Figure 6f, Figure 6g, 740 ± 12 to 910 ± 16, and Supplementary Information Movie S3), suggesting that the DUB fusion did not sterically inhibit endocytic dynamics. Importantly, the fraction of short-lived endocytic events in cells expressing each of the CRY2 chimeras was similar to that in Eps15 knockout cells, suggesting that expression of Eps15-CRY2-DUB did not significantly impact endocytic dynamics prior to its light-activated recruitment to endocytic sites. Taken together, these results suggest that loss of ubiquitylation acutely destabilizes endocytic sites within minutes.

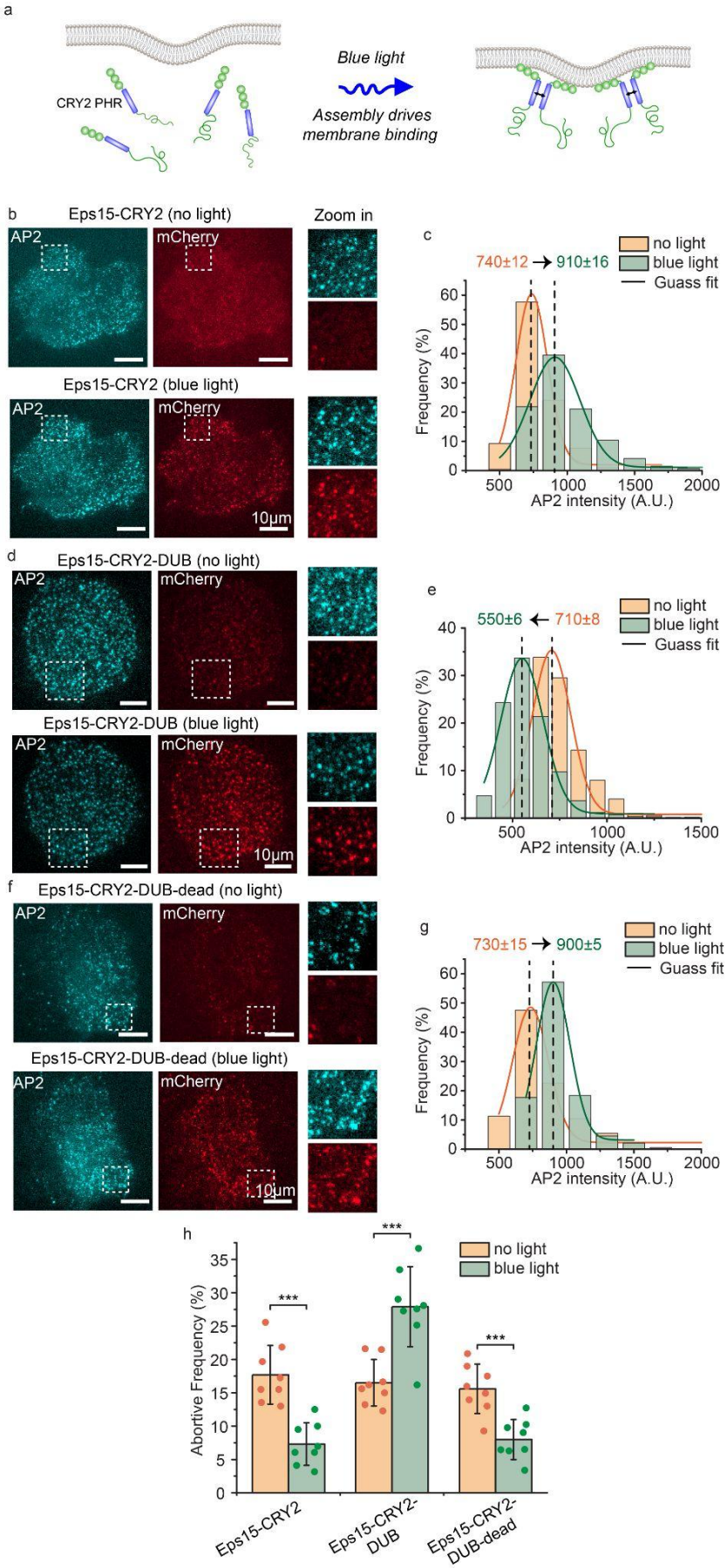
a
CRY2 PHR
Blue light
Assembly drives membrane binding
b
Eps15-CRY2 (no light)
Zoom in
AP2
mCherry
Eps15-CRY2 (blue light)
10μm
c
740±12 → 910±16
no light
blue light
Guass fit
Frequency (%)
AP2 intensity (A.U.)
d
Eps15-CRY2-DUB (no light)
Eps15-CRY2-DUB (blue light)
e
550±6 ← 710±8
f
Eps15-CRY2-DUB-dead (no light)
Eps15-CRY2-DUB-dead (blue light)
g
730±15 → 900±5
h
Abortive Frequency (%)
***
Eps15-CRY2
Eps15-CRY2-DUB
Eps15-CRY2-DUB-dead

Figure 6. Light-activated recruitment of DUBs demonstrates that loss of ubiquitination destabilizes endocytic sites within minutes. a, Schematic of blue light driving assembly and membrane binding of Eps15-CRY2 chimera in which the Eps15 coiled-coil domain is replaced with the light-activation CRY2 PHR domain. **b, d, f**, Representative images of Eps15KO SUM cells expressing Eps15-CRY2 (**b**), Eps15-CRY2-DUB (**d**) and Eps15-CRY2-DUB-dead (**f**) before and after applying blue light. AP-2 σ2-HaloTag was labeled with JF646 (cyan). Insets show the zoom-in area of the white dashed box. mCherry was fused to all three constructs at their C terminus for visualization. Scale bar = 10 μm. **c, e, g**, Histograms and the Guass fit of the AP2 intensity distribution tracked in endocytic pits when expressing Eps15-CRY2 (**c**), Eps15-CRY2-DUB (**e**) and Eps15-CRY2-DUB-dead (**g**) before and after exposed to blue light, repectively. **h**, Frequency of short-lived structures comparison before and after blue light was applied to the cells under each condition. For Eps15-CYR2, n = 8 biologically independent cell samples were collected and in total 1060 pits (before light) and 1068 pits (blue light) were analyzed. For Eps15-CRY2-DUB, n = 8 and 1099 pits (before light) and 1371 pits (blue light) were analyzed. For Eps15-CRY2-DUB-dead, n = 8 and total pits = 1044 (before light) and 918 (blue light). Dots represent frequecy from each sample. An unpaired, two-tailed student's t test was used for statistical significance. ***: $P < 0.001$. Error bars represent standard deviation. Cells were imaged at 37°C for all conditions.

Discussion

Here we demonstrate that ubiquitylation plays an important role in stabilizing the flexible network of early initiator proteins during clathrin-mediated endocytosis. *In vitro* experiments with protein droplets and giant unilamellar vesicles collectively demonstrated that polyubiquitin, but not monoubiquitin, is strongly recruited to liquid-like networks of the initiator protein, Eps15. Importantly, these effects required Eps15's ubiquitin interacting motif (UIM). Similarly, in live cell imaging experiments, a version of Eps15 lacking the UIM domain failed to rescue the increase in short-lived endocytic structures resulting from Eps15 knockout. These results suggest that interactions between Eps15 and ubiquitylated proteins, either transmembrane cargo or other endocytic proteins, can stabilize the early endocytic network. Testing this idea *in vitro*, we found that the melting temperature of the Eps15 network increased substantially in the presence of polyubiquitin, but not monoubiquitin, an effect which required Eps15's UIM domain. To test the impact of ubiquitin on the stability of endocytic sites more broadly, we next evaluated the impact of deubiquitinase (DUB) enzymes on coated vesicle dynamics. Here we found that expressing a version of Eps15 fused to a broad-spectrum DUB approximately doubled the number of unstable, short-lived endocytic sites, rather than rescuing the defect created by Eps15 knockout. Further, by using a light activated recruitment system for Eps15-DUB, we demonstrated that loss of ubiquitin can acutely destabilize endocytic sites within minutes, a result which likely represents the cumulative effect of removing ubiquitin from multiple endocytic proteins and transmembrane protein cargos.

Our finding that polyubiquitin can stabilize early endocytic networks is supported by earlier work suggesting the importance of ubiquitylation in endocytosis. Specifically, the early initiator protein, Eps15, and the adaptor protein, Epsin, are both known to contain UIM motifs[18,45]. Epsin, in particular, is thought to act as a cargo adaptor for ubiquitinated transmembrane proteins[9,45,46]. Interestingly, Eps15 and Epsin interact through binding between Eps15's EH domains and Epsin's NPF (asparagine, proline, phenylalanine) domain, suggesting that they may be key components within a ubiquitin-stabilized protein network that facilities efficient endocytosis[47,48].

Similarly, prior work in budding yeast cells suggests that mono- and poly-ubiquitylated transmembrane proteins contribute to the stability of endocytic sites. Specifically, attachment of K63-linked polyubiquitin chains to permeases at the plasma membrane significantly accelerated their internalization by the clathrin pathway[21]. Further, conjugation of cargo proteins with polyubiquitin chains promoted more efficient endocytosis than conjugation with monoubiquitin[49]. Additionally, endogenous deubiquitinases (DUBs) were found to play a critical role in the turnover of endocytic sites, avoiding overly stable, long-lived sites that become stalled[23]. While the role of ubiquitination in mammalian cell endocytosis has been less explored, ubiquitination of receptors is known to be important for Epsin-mediated uptake of influenza virus by the clathrin pathway[43].

In the context of this literature, our work suggests that a key role of ubiquitylation is to stabilize the early endocytic network, such that endocytic sites mature efficiently into productive coated vesicles (Figure 5e). Specifically, an increase or decrease in ubiquitination at endocytic sites, which cells could achieve by modulating ubiquitylation of endocytic proteins or transmembrane cargos, could effectively modulate endocytic dynamics. Prior work on endocytic dynamics has suggested that nascent endocytic sites mature into productive endocytic structures by passing through a series of biochemical "checkpoints" or criteria, the precise identity of which remains unknown[1]. In this context, our results suggest that the ubiquitin content of endocytic sites, which stabilizes the flexible network of early endocytic proteins, may constitute such a checkpoint.

Materials and Methods

Reagents

Tris-HCl (Tris hydrochloride), HEPES (4-(2-hydroxyethyl)-1-piperazineethanesulfonic acid), IPTG (isopropyl-β-D-thiogalactopyranoside), NaCl, β-mercaptoethanol, Triton X-

100, neutravidin, and Texas Red-DHPE (Texas Red 1,2-dihexadecanoyl-sn-glycero-3-phosphoethanolamine triethylammonium salt) were purchased from Thermo Fisher Scientific. Sodium bicarbonate, sodium tetraborate, EDTA (Ethylene diamine tetraacetic acid), EGTA (Ethylene glycol tetraacetic acid), glycerol, TCEP (tris(2-carboxyethyl) phosphine), DTT (Dithiothreitol), PMSF (phenylmethanesulfonylfluoride), EDTA-free protease inhibitor tablets, thrombin, imidazole, sodium bicarbonate, PLL (poly-l-lysine), Atto640 NHS ester and Atto488 NHS ester were purchased from Sigma-Aldrich. Monoubiquitin and K63 linked Tetraubiquitin were purchased from Boston Biochem (Catalog #: U-100H and UC-310). PEG 8000 (Polyethylene glycol 8000) was purchased from Promega (Catalog #: V3011). Amine-reactive PEG (mPEG-succinimidyl valerate MW 5000) and PEG-biotin (Biotin-PEG SVA, MW 5000) were purchased from Laysan Bio. DP-EG10-biotin (dipalmitoyl-decaethylene glycol-biotin) was provided by D. Sasaki (Sandia National Laboratories). POPC (1-palmitoyl-2-oleoyl-glycero-3-phosphocholine) and DGS-NTA-Ni (1,2-dioleoyl-sn-glycero-3-[(N-(5-amino-1-carboxypentyl) iminodiacetic acid)-succinyl] (nickel salt)) were purchased from Avanti Polar Lipids. All reagents were used without further purification.

Plasmids

Plasmids used for purifying Eps15 and Eps15ΔUIM from bacteria are pET28a-6×His-Eps15 (FL) and pET28a-6×His-Eps15ΔUIM. pET28a-6×His-Eps15 (FL) encoding H. sapiens Eps15 was kindly provided by T. Kirchhausen[25], Harvard Medical School, USA. pET28a-6×His-Eps15ΔUIM was generated by using site-directed mutagenesis to introduce a stop codon after residue 850 of Eps15 to generate a truncated version lacking residues 851-896 corresponding to the UIM domains at the C terminus. The forward primer 5'-GTGCTTATCCCTGAGAAGAAGATATGATCG-3' and reverse primer 5'-CATATCTTCTTCTCAGGGATAAGCACTGAAG-3' were used.

Plasmids used for mammalian cell expression of Eps15 variants were derived from Eps15-pmCherryN1 (Addgene plasmid #27696, a gift from C. Merrifield[50]), which encodes Eps15-mCherry (denoted as Eps15wt). All of the following Eps15 variants contain mCherry at their C terminal end for visualization even though mCherry is not mentioned in their names. The Eps15ΔUIM plasmid was generated by PCR-mediated deletion of the UIM domains (residues 851-896). The 138 base pairs corresponding to the two UIM domains were deleted using the 5' phosphorylated forward primer 5'-CGGATGGGTTCGACCTC-3' and the reverse primer 5'-GGGATAAGCACTGAAGTTGG-3'. After PCR amplification and purification, the PCR product was recircularized to generate the Eps15ΔUIM. Plasmids encoding the broad-spectrum deubiquitinase (DUB), UL36, and the catalytically inert mutant (C56S, DUB-dead), were generously provided by J. A. MacGurn[38]. Plasmids encoding the Eps15-DUB

and Eps15-DUB-dead were generated by restriction cloning. Amplification of the DUB and DUB-dead was achieved using the forward primer 5'-CATGAGGATCCAATGGACTACAAAGACCATGACG-3' and the reverse primer 5'-CATGAGGATCCGGGTATGGGTAAAAGATGCGG-3'. The amplicon was then inserted into the Eps15-pmCherryN1 at the BamH1 restriction sites between Eps15 and mCherry. The plasmid encoding Eps15-CRY2 was generated by using the crytochrome 2 photolyase homology region (CRY2 PHR) domain of *Arabidopsis thaliana* to replace the coiled-coil domain in Eps15 based on our previous report[12]. Specifically, the CRY2 PHR domain was PCR amplified from pCRY2PHR-mCherryN1 (Addgene plasmid #26866, a gift from C. Tucker[51]) using primers 5′-TAGGATCAAGTCCTGTTGCAGCCACCATGAAGATGGACAAAAAGAC-3′ and 5′-ATCAGTTTCATTTGCATTGAGGCTGCTGCTCCGATCAT-3′. This fragment was inserted by Gibson assembly (New England Biolabs) into Eps15-pmCherryN1 (Addgene plasmid#27696, a gift from C. Merrifield2), which were PCR amplified to exclude Eps15 coiled-coil domain (residues 328–490) using primers 5′-TCATGATCGGAGCAGCAGCCTCAATGCAAATGAAACTGATGGAAATGAAAGATTTG GAAAATCATAATAG-3′ and 5′-TTGTCCATCTTCATGGTGGCTGCAACAGGACTTGATCCTATGAT-3′. Plasmids encoding Eps15-CRY2-DUB and Eps15-CRY2-DUB-dead were generated by inserting DUB and DUB-dead in between Eps15-CRY2 and mCherry through Gibson assembly. The primers 5'-GTCAGCTGGCCCGGGATCCAATGGACTACAAA-3' and 5'-CTCACCATGGTGGCGACCGGTGGATCCGGGTA-3' were used for amplifying DUB and DUB-dead and primers 5'-TTTACCCATACCCGGATCCACCGGTCGCCACCA-3' and 5'-TCATGGTCTTTGTAGTCCATTGGATCCCGGGCCAG-3' were used for amplifying the vector Eps15-CRY2.

All constructs were confirmed by DNA sequencing.

Protein purification

Eps15 and Eps15ΔUIM were purified based on a previously reported protocol[12]. Briefly, full-length Eps15 and Eps15ΔUIM were expressed as N-terminal 6×His-tagged constructs in BL21 (DE3) Escherichia coli cells. Cells were grown in 2×YT medium for 3-4 h at 30 °C to an optical density at 600 nm of 0.6-0.9, then protein expression was induced with 1 mM IPTG at 30 °C for 6-8 hours. Cells were collected, and bacteria were lysed in lysis buffer using homogenization and probe sonication on ice. Lysis buffer consisted of 20 mM Tris-HCl, pH 8.0, 300 mM NaCl, 5% glycerol, 10 mM imidazole, 1 mM TCEP, 1 mM PMSF, 0.5% Triton X-100 and 1 EDTA-free protease inhibitor cocktail tablet (Roche: Cat#05056489001) per 50 mL buffer. Proteins were incubated with Ni-NTA Agarose (Qiagen, Cat#30230) resin for 30 min at 4 °C in a beaker with stirring, followed

by extensive washing with 10 column volumes of lysis buffer with 20 mM imidazole and 0.2% Triton X-100 and 5 column volumes of buffer without Triton X-100. Then proteins were eluted from the resin in 20 mM Tris-HCl, pH 8.0, 300 mM NaCl, 5% glycerol, 250 mM imidazole, 0.5 mM TCEP, 1 mM PMSF, and EDTA-free protease inhibitor cocktail tablet. Eluted proteins were further purified by gel filtration chromatography using a Superose 6 column run in 20 mM Tris-HCl, pH 8.0, 150 mM NaCl, 1 mM EDTA, and 5 mM DTT. For droplet experiments, prior to running the gel filtration column, the 6×His tag on the proteins was further cleaved with Thrombin CleanCleave kit (Sigma-Aldrich, Cat# RECMT) overnight at 4 °C on the rocking table after desaltig in 50 mM Tris-HCl, pH 8.0, 10 mM $CaCl_2$, 150 mM NaCl and 1 mM EDTA using a Zeba Spin desalting column (Thermo Scientific, Cat#89894). The purified proteins were dispensed into small aliquots, flash frozen in liquid ntitrogen and stored at -80 °C.

Protein labeling

Eps15 and Eps15ΔUIM were labeled with amine-reactive NHS ester dyes Atto488 in phosphate-buffered saline (PBS, Hyclone) containing 10 mM sodium bicarbonate, pH 8.3. Monoubiquitin and tetraubiquitin were labeled with Atto640 in PBS, pH 7.4. The concentration of dye was adjusted experimentally to obtain a labeling ratio of 0.5–1 dye molecule per protein, typically using 2-fold molar excess of dye. Reactions were performed for 30 min on ice. Then labeled Eps15 and Eps15ΔUIM was buffer exchanged into 20 mM Tris-HCl pH 7.5, 150 mM NaCl, 5 mM TCEP, 1 mM EDTA, 1 mM EGTA and separated from unconjugated dye using Princeton CentriSpin-20 size-exclusion spin columns (Princeton Separations). The labeled monoubiquitin and tetraubiquitin were buffer exchanged to 20 mM Tris-HCl, 150 mM NaCl, pH 7.5 and separated from unconjugated dye as well using 3K Amicon columns. Labeled proteins were dispensed into small aliquots, flash frozen in liquid nitrogen and stored at -80°C. For all experiments involving labeled Eps15 and Eps15ΔUIM, a mix of 90% unlabelled/10% labeled protein was used. 100% labeled monoubiquitin and tetraubiquitin were directly used due to their small fraction compared to Eps15 variants.

PLL-PEG preparation

PLL-PEG and biotinylated PLL-PEG were prepared as described previously with minor alterations[52]. Briefly, for PLL-PEG, amine-reactive mPEG-succinimidyl valerate was mixed with poly-L-lysine (15–30 kD) at a molar ratio of 1:5 PEG to poly-L-lysine. For biotinylated PLL-PEG, amine reactive PEG and PEG-biotin was first mixed at a molar ratio of 98% to 2%, respectively, and then mixed with PLL at 1:5 PEG to PLL molar ratio. The conjugation reaction was performed in 50 mM sodium tetraborate pH 8.5 solution and allowed to react overnight at room temperature with continued stirring. The products were

buffer exchanged into 5 mM HEPES, 150 mM NaCl pH 7.4 using Zeba spin desalting columns (7K MWCO, ThermoFisher) and stored at 4 °C.

Protein droplets

Eps15 or Eps15ΔUIM droplets were formed by mixing proteins with 3% w/v PEG8000 in 20 mM Tris-HCl pH 7.5, 150 mM NaCl, 5 mM TCEP 1 mM EDTA, 1 mM EGTA. 7 μM Eps15 or Eps15ΔUIM was used to form the droplets, with addition of ubiquitins accordingly. For imaging droplets, 2% PLL-PEG were used to passivate coverslips (incubated for 20 min) before adding protein-containing solutions. Imaging wells consisted of 5 mm diameter holes in 0.8 mm thick silicone gaskets (Grace Bio-Labs). Gaskets were placed directly onto no.1.5 glass coverslips (VWR International), creating a temporary water-proof seal. Prior to well assembly, gaskets and cover slips were cleaned in 2% v/v Hellmanex III (Hellma Analytics) solution, rinsed thoroughly with water, and dried under a nitrogen stream. The imaging well was washed 6-8 times with 20 mM Tris-HCl, 150 mM NaCl and 5 mM TCEP buffer before adding solutions that contained proteins.

GUV preparation

GUVs consisted of 93 mol% POPC, 5 mol% Ni-NTA, and 2 mol% DP-EG10 biotin. GUVs were prepared by electroformation according to published protocols[53]. Briefly, lipid mixtures dissolved in chloroform were spread into a film on indium-tin-oxide (ITO) coated glass slides (resistance ~8-12 W per square) and further dried in a vacuum desiccator for at least 2 hours to remove all of the solvent. Electroformation was performed at 55°C in glucose solution with an osmolarity that matched the buffer to be used in the experiments. The voltage was increased every 3 min from 50 to 1400 mV peak to peak for the first 30 min at a frequency of 10 Hz. The voltage was then held at 1400 mV peak to peak, 10 Hz, for 120 min and finally was increased to 2200 mV peak to peak, for the last 30 min during which the frequency was adjusted to 5 Hz. GUVs were stored in 4°C and used within 3 days after electroformation.

GUV tethering

GUVs were tethered to glass coverslips for imaging as previously described[28]. Briefly, glass cover slips were passivated with a layer of biotinylated PLL-PEG, using 5 kDa PEG chains. GUVs doped with 2 mol% DP-EG10-biotin were then tethered to the passivated surface using neutravidin. Imaging wells consisted of 5 mm diameter holes in 0.8 mm thick silicone gaskets were prepared by placing silicone gaskets onto Hellmanex III cleaned coverslips. In each imaging well, 20 μL of biotinylated PLL-PEG was added. After 20 min of incubation, wells were serially rinsed with appropriate buffer by gently pipetting

until a 15,000-fold dilution was achieved. Next, 4 μg of neutravidin dissolved in 25 mM HEPES, 150 mM NaCl (pH 7.4) was added to each sample well and allowed to incubate for 10 minutes. Wells were then rinsed with the appropriate buffer to remove excess neutravidin. GUVs were diluted in 20 mM Tris-HCl, 150 mM NaCl, 5 mM TCEP, pH 7.5 at ratio of 1:13 and then 20 μL of diluted GUVs was added to the well and allowed to incubate for 10 minutes. Excess GUVs were then rinsed from the well using the same buffer and the sample was subsequently imaged using confocal fluorescence microscopy.

Cell culture

Human-derived SUM159 cells gene-edited to add a HaloTag to both alleles of AP-2 σ2 were a gift from T. Kirchhausen[54]. Cells were further gene-edited to knock out both alleles of endogenous Eps15 using CRISPR-associated protein 9 (Cas9) to produce the Eps15 knockout cells developed previously by our group[12].

Cells were grown in 1:1 DMEM high glucose: Ham's F-12 (Hyclone, GE Healthcare) supplemented with 5% fetal bovine serum (Hyclone), Penicillin/Streptomycin/l-glutamine (Hyclone), 1 μg ml^{-1} hydrocortisone (H4001; Sigma-Aldrich), 5 μg ml^{-1} insulin (I6634; Sigma-Aldrich) and 10 mM HEPES, pH 7.4 and incubated at 37 °C with 5% CO_2. Cells were seeded onto acid-washed coverslips at a density of 3×10^4 cells per coverslip for 24 h before transfection with 1μg of plasmid DNA using 3 μl Fugene HD transfection reagent (Promega). HaloTagged AP-2 σ2 was visualized by adding Janelia Fluor 646-HaloTag ligand (Promega). Ligand (100 nM) was added to cells and incubated at 37 °C for 15 min. Cells were washed with fresh medium and imaged immediately.

Fluorescence microscopy

Images of protein droplets and GUVs were collected on a spinning disc confocal super resolution microscope (SpinSR10, Olympus, USA) equipped with a 1.49 NA/100X oil immersion objective. For GUV imaging, image stacks taken at fixed distances perpendicular to the membrane plane (0.5 μm steps) were acquired immediately after GUV tethering and again after protein addition. Images taken under deconvolution mode were processed by the built-in deconvolution function in Olympus CellSens software (Dimension 3.2, Build 23706). At least 30 fields of views were randomly selected for each sample for further analysis. Imaging was performed 5 min after adding proteins, providing sufficient time to achieve protein binding and reach a steady state level of binding. For experiments used to construct phase diagrams, temperature was monitored by a thermistor placed in the protein solution in a sealed chamber to prevent evaporation. Samples were heated from room temperature through an aluminum plate fixed to the top of the chamber. Temperature was increased in steps of 1 °C until the critical temperature

was reached. Images of at least 20 droplets were taken at each temperature, once the temperature stabilized.

Live-cell images were collected on a TIRF microscope consisting of an Olympus IX73 microscope body, a Photometrics Evolve Delta EMCCD camera, and an Olympus 1.4 NA ×100 Plan-Apo oil objective, using MicroManager version 1.4.23. The coverslip was heated to produce a sample temperature of 37 °C using an aluminum plate fixed to the back of the sample. All live-cell imaging was conducted in TIRF mode at the plasma membrane 48 h after transfection. Transfection media used for imaging lacked pH indicator (phenol red) and was supplemented with 1 μL OxyFluor (Oxyrase, Mansfield, OH) per 33 μL media to decrease photobleaching during live-cell fluorescence imaging. 532 nm and 640 nm lasers were used for excitation of mCherry and Janelia Fluor 646-HaloTag ligand of AP2, respectively. Cell movies were collected over 10 min at 2 s intervals between frames. For blue-light assays, samples were exposed to 25 μW 473 nm light as measured out of the objective when in wide-field mode. Blue light was applied for 500 ms every 3 s for cell samples. Cell movies were collected over 11 min at 3 s intervals between frames, and analysis of movies began after 1 min of imaging to allow for blue light to take effect.

Image analysis

Fluorescence images analyzed in ImageJ (http://rsbweb.nih.gov/ij/). Intensity values along line scans were measured in unprocessed images using ImageJ. For phase diagrams, fluorescence intensity was measured in the center square of a 3 × 3 grid for each image where illumination was even. Two images were analyzed at each temperature for each condition. The intensity was normalized to the mean intensity value of the solution (200 A.U.).

Clathrin-coated structures were detected and tracked using cmeAnalysis in MATLAB[55]. The point spread function of the data was used to determine the standard deviation of the Gaussian function. AP-2 σ2 signal was used as the master channel to track clathrin-coated structures. Detected structures were analyzed if they persisted in at least three consecutive frames. The lifetimes of clathrin-coated that met these criteria were recorded for lifetime distribution analysis under different conditions.

Statistical analysis

For all experiments yielding micrographs, each experiment was repeated independently on different days at least three times, with similar results. Phase diagram experiments

were repeated independently twice with similar results. Collection of cell image data for clathrin-mediated endocytosis analysis was performed independently on at least two different days for each cell type or experimental condition. Statistical analysis was carried out using Welch's t-tests (unpaired, unequal variance) to probe for statistical significance ($P < 0.05$).

Supplementary Information

Movie S1: Eps15 droplets fusion with addition of MonoUb. Eps15 (7μM) droplets (green) were incubated with 1μM MonoUb (magenta) in 20 mM Tris-HCl, 150 mM NaCl, 5 mM TCEP, 1 mM EDTA and 1 mM EGTA at pH 7.5 with 3% w/v PEG8000.

Movie S2: Eps15 droplets fusion with addition of TetraUb. Eps15 (7μM) droplets (green) were incubated with 0.25μM K63 linkage TetraUb (magenta) in 20 mM Tris-HCl, 150 mM NaCl, 5 mM TCEP, 1 mM EDTA and 1 mM EGTA at pH 7.5 with 3% w/v PEG8000.

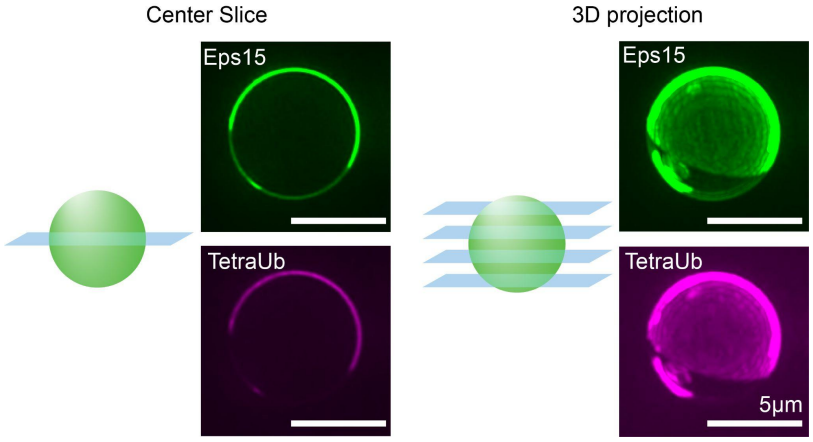

Figure S1. Centre slices (left) and corresponding z-projections (right) of representative images of Eps15 (green) assembled into protein condensed region together with TetraUb (magenta) on GUV membrane. GUVs were incubated with 0.5 μM Eps15 and 0.2 μM TetraUb in 20 mM Tris-HCl pH 7.5, 150 mM NaCl, 5 mM TCEP buffer. Scale bar = 5 μm.

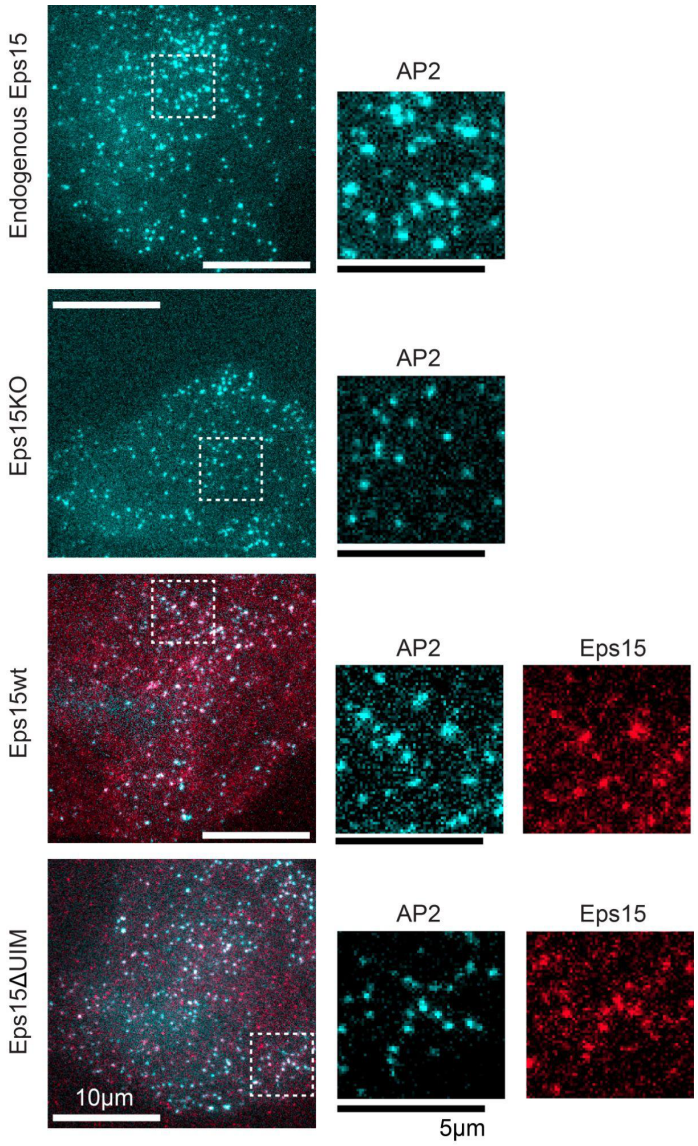

Figure S2. Representative image of endocytic pits in live SUM cells expressing gene-edited AP2 σ2-HaloTag: JF646 (cyan) and Eps15 variants (red). Endogenous Eps15 represents SUM cells expressing gene-edited AP2 σ2-HaloTag. Eps15KO represents SUM cells that were further CRISPR modified to knockout alleles of endogenous Eps15. Eps15wt and Eps15ΔUIM represent Eps15KO cells transfected with wildtype Eps15 and Eps15 with the depletion of both UIM domains, respectively. mCherry was fused to the C terminus of Eps15 and Eps15ΔUIM for visualization. Insets are the zoom-in area of the white dashed box. Scale bars are labeled in images. Cells were imaged at 37°C for all conditions.

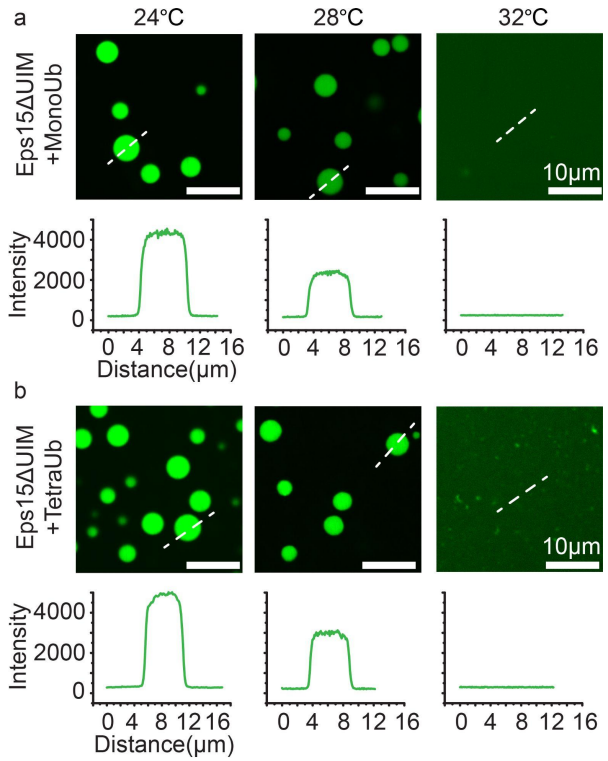

Figure S3. Representative images of protein droplets at increasing temperatures. Plots show fluorescence intensity of Eps15ΔUIM measured along dotted lines in each image. Droplets are formed from (**a**) 0.5 μM MonoUb, 7 μM Eps15ΔUIM and (**b**) 0.1 μM TetraUb, 7 μM Eps15ΔUIM in 20 mM Tris-HCl, 150 mM NaCl, 5 mM TCEP, 1 mM EDTA and 1 mM EGTA at pH 7.5 buffer with 3% PEG8000. Scale bars equal 10 μm.

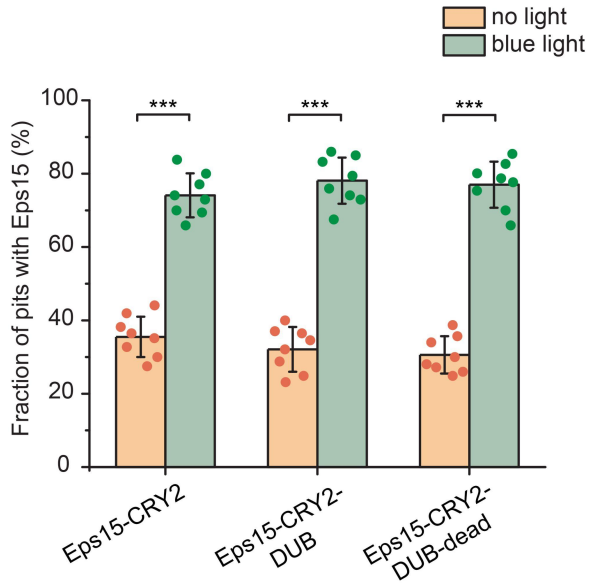

Figure S4. Fraction of endocytic pits showing Eps15 colocalization before and after exposure to blue light when expressing Eps15-CRY2, Eps15-CRY2-DUB, or Eps15-CRY2-DUB-dead. For Eps15-CYR2, n = 8 biologically independent cell samples were collected and in total 1060 pits (before light) and 1068 pits (blue light) were analyzed. For Eps15-CRY2-DUB, n = 8 and 1099 pits (before light) and 1371 pits (blue light) were analyzed. For Eps15-CRY2-DUB-dead, n = 8 and total pits = 1044 (before light) and 918 (blue light). Dots represent frequency from each sample. An unpaired, two-tailed student's t test was used for statistical significance. ***: $P < 0.001$. Error bars represent standard deviation. Cells were imaged at 37°C for all conditions.

Movie S3: Change of Eps15 and AP2 channel upon light activation in cells expressing Eps15-CRY2, Eps15-CRY2-DUB and Eps15-CRY2-DUB-dead, respectively.

Acknowledgements

We thank T. Kirchhausen for the gift of SUM159/AP2-σ2-Halo Tag cells and J. MacGurn for the gift of plasmids encoding deubiquitinase UL36 and its catalytically inactive mutant. This research was supported by the National Institutes of Health through grants R35GM139531 to J.C.S., the Welch Foundation through grant F-2047 to J.C.S., and the University of Texas at Austin, Graduate School Continuing Fellowship 2022-2023 to F.Y.

Author contributions

F.Y., K.J.D., J.M.H., and J.C.S. designed the experiments. L.W. and E.M.L. purified Eps15 and the variants for *in vitro* experiments. F.Y., A.S. and B.T.M conducted the *in vitro* experiments. F.Y., S.G., and A.S. performed the cloning and cell assays. F.Y., S.G., G.A., and J.C.S. contributed to data analysis. F.Y., L.W., E.M.L., J.M.H., and J.C.S. wrote the paper. All authors consulted on manuscript preparation and editing.

Competing interests

The authors declare no competing interests.

Data availability

All data supporting this work are available on request from corresponding author. CMEanalysis codes are available here:

https://www.utsouthwestern.edu/labs/danuser/software/. No custom code was generated for this study.

References

1. Mettlen, M., Chen, P.-H., Srinivasan, S., Danuser, G. & Schmid, S. L. Regulation of Clathrin-Mediated Endocytosis. *Annual Review of Biochemistry* vol. 87 871–896 (2018).
2. McMahon, H. T. & Boucrot, E. Molecular mechanism and physiological functions of clathrin-mediated endocytosis. *Nat. Rev. Mol. Cell Biol.* **12**, 517–533 (2011).
3. Kaksonen, M. & Roux, A. Mechanisms of clathrin-mediated endocytosis. *Nat. Rev. Mol. Cell Biol.* **19**, 313–326 (2018).
4. Chen, Z. & Schmid, S. L. Evolving models for assembling and shaping clathrin-coated pits. *J. Cell Biol.* **219**, e202005126 (2020).
5. Traub, L. M. Tickets to ride: selecting cargo for clathrin-regulated internalization. *Nat. Rev. Mol. Cell Biol.* **10**, 583–596 (2009).
6. Hicke, L. & Riezman, H. Ubiquitination of a yeast plasma membrane receptor signals its ligand-stimulated endocytosis. *Cell* **84**, 277–287 (1996).
7. Galan, J. M., Moreau, V., Andre, B., Volland, C. & Haguenauer-Tsapis, R. Ubiquitination Mediated by the Npi1p/Rsp5p Ubiquitin-protein Ligase Is Required for Endocytosis of the Yeast Uracil Permease (∗). *J. Biol. Chem.* **271**, 10946–10952 (1996).
8. Lin, C. H., MacGurn, J. A., Chu, T., Stefan, C. J. & Emr, S. D. Arrestin-related ubiquitin-ligase adaptors regulate endocytosis and protein turnover at the cell surface. *Cell* **135**, 714–725 (2008).
9. Dores, M. R., Schnell, J. D., Maldonado-Baez, L., Wendland, B. & Hicke, L. The function of yeast epsin and Ede1 ubiquitin-binding domains during receptor internalization. *Traffic* **11**, 151–160 (2010).

10. Tebar, F., Sorkina, T., Sorkin, A., Ericsson, M. & Kirchhausen, T. Eps15 is a component of clathrin-coated pits and vesicles and is located at the rim of coated pits. *J. Biol. Chem.* **271**, 28727–28730 (1996).

11. Sochacki, K. A., Dickey, A. M., Strub, M.-P. & Taraska, J. W. Endocytic proteins are partitioned at the edge of the clathrin lattice in mammalian cells. *Nat. Cell Biol.* **19**, 352–361 (2017).

12. Day, K. J. *et al.* Liquid-like protein interactions catalyse assembly of endocytic vesicles. *Nat. Cell Biol.* **23**, 366–376 (2021).

13. Wilfling, F. *et al.* A selective autophagy pathway for phase-separated endocytic protein deposits. *Mol. Cell* **80**, 764-778. e7 (2020).

14. Wilfling, F., Lee, C.-W., Erdmann, P. S. & Baumeister, W. Autophagy ENDing unproductive phase-separated endocytic protein deposits. *Autophagy* **17**, 3264–3265 (2021).

15. Kozak, M. & Kaksonen, M. Condensation of Ede1 promotes the initiation of endocytosis. *Elife* **11**, e72865 (2022).

16. Shih, S. C. *et al.* Epsins and Vps27p/Hrs contain ubiquitin-binding domains that function in receptor endocytosis. *Nat. Cell Biol.* **4**, 389–393 (2002).

17. Hicke, L. & Dunn, R. Regulation of membrane protein transport by ubiquitin and ubiquitin-binding proteins. *Annu. Rev. Cell Dev. Biol.* **19**, 141–172 (2003).

18. Polo, S. *et al.* A single motif responsible for ubiquitin recognition and monoubiquitination in endocytic proteins. *Nature* **416**, 451–455 (2002).

19. Riezman, H. The ubiquitin connection. *Nature* **416**, 381–383 (2002).

20. Weinberg, J. S. & Drubin, D. G. Regulation of clathrin-mediated endocytosis by dynamic ubiquitination and deubiquitination. *Curr. Biol.* **24**, 951–959 (2014).

21. Galan, J.-M. & Haguenauer-Tsapis, R. Ubiquitin lys63 is involved in ubiquitination of a yeast plasma membrane protein. *EMBO J.* **16**, 5847–5854 (1997).

22. Huang, F. *et al.* Lysine 63-linked polyubiquitination is required for EGF receptor degradation.

Proc. Natl. Acad. Sci. **110**, 15722–15727 (2013).

23. Erpapazoglou, Z., Walker, O. & Haguenauer-Tsapis, R. Versatile roles of k63-linked ubiquitin chains in trafficking. *Cells* **3**, 1027–1088 (2014).
24. Piper, R. C., Dikic, I. & Lukacs, G. L. Ubiquitin-dependent sorting in endocytosis. *Cold Spring Harb. Perspect. Biol.* **6**, a016808 (2014).
25. Cupers, P., ter Haar, E., Boll, W. & Kirchhausen, T. Parallel dimers and anti-parallel tetramers formed by epidermal growth factor receptor pathway substrate clone 15 (EPS15). *J. Biol. Chem.* **272**, 33430–33434 (1997).
26. Benmerah, A., Poupon, V., Cerf-Bensussan, N. & Dautry-Varsat, A. Mapping of Eps15 domains involved in its targeting to clathrin-coated pits. *J. Biol. Chem.* **275**, 3288–3295 (2000).
27. Santonico, E., Panni, S., Falconi, M., Castagnoli, L. & Cesareni, G. Binding to DPF-motif by the POB1 EH domain is responsible for POB1-Eps15 interaction. *BMC Biochem.* **8**, 1–14 (2007).
28. Yuan, F. *et al.* Membrane bending by protein phase separation. *Proc. Natl. Acad. Sci.* **118**, e2017435118 (2021).
29. Lu, R. & Drubin, D. G. Selection and stabilization of endocytic sites by Ede1, a yeast functional homologue of human Eps15. *Mol. Biol. Cell* **28**, 567–575 (2017).
30. Ehrlich, M. *et al.* Endocytosis by random initiation and stabilization of clathrin-coated pits. *Cell* **118**, 591–605 (2004).
31. Boulant, S., Kural, C., Zeeh, J.-C., Ubelmann, F. & Kirchhausen, T. Actin dynamics counteract membrane tension during clathrin-mediated endocytosis. *Nat. Cell Biol.* **13**, 1124–1131 (2011).
32. Collins, B. M., McCoy, A. J., Kent, H. M., Evans, P. R. & Owen, D. J. Molecular architecture and functional model of the endocytic AP2 complex. *Cell* **109**, 523–535 (2002).
33. Owen, D. J., Collins, B. M. & Evans, P. R. Adaptors for clathrin coats: structure and function.

Annu Rev Cell Dev Biol **20**, 153–191 (2004).

34. Grimm, J. B. *et al.* A general method to improve fluorophores for live-cell and single-molecule microscopy. *Nat. Methods* **12**, 244–250 (2015).
35. Blondeau, F. *et al.* Tandem MS analysis of brain clathrin-coated vesicles reveals their critical involvement in synaptic vesicle recycling. *Proc. Natl. Acad. Sci.* **101**, 3833–3838 (2004).
36. Dao, T. P. *et al.* Mechanistic insights into enhancement or inhibition of phase separation by different polyubiquitin chains. *EMBO Rep.* **23**, e55056 (2022).
37. Stringer, D. K. & Piper, R. C. A single ubiquitin is sufficient for cargo protein entry into MVBs in the absence of ESCRT ubiquitination. *J. Cell Biol.* **192**, 229–242 (2011).
38. Xu, P. *et al.* COPI mediates recycling of an exocytic SNARE by recognition of a ubiquitin sorting signal. *Elife* **6**, e28342 (2017).
39. Nielsen, C. P., Jernigan, K. K., Diggins, N. L., Webb, D. J. & MacGurn, J. A. USP9X deubiquitylates DVL2 to regulate WNT pathway specification. *Cell Rep.* **28**, 1074-1089. e5 (2019).
40. Kattenhorn, L. M., Korbel, G. A., Kessler, B. M., Spooner, E. & Ploegh, H. L. A deubiquitinating enzyme encoded by HSV-1 belongs to a family of cysteine proteases that is conserved across the family Herpesviridae. *Mol. Cell* **19**, 547–557 (2005).
41. Bolstad, M., Abaitua, F., Crump, C. M. & O'Hare, P. Autocatalytic activity of the ubiquitin-specific protease domain of herpes simplex virus 1 VP1-2. *J. Virol.* **85**, 8738–8751 (2011).
42. Komander, D. & Rape, M. The ubiquitin code. *Annu. Rev. Biochem.* **81**, 203–229 (2012).
43. Chen, C. & Zhuang, X. Epsin 1 is a cargo-specific adaptor for the clathrin-mediated endocytosis of the influenza virus. *Proceedings of the National Academy of Sciences* vol. 105 11790–11795 (2008).
44. Bugaj, L. J., Choksi, A. T., Mesuda, C. K., Kane, R. S. & Schaffer, D. V. Optogenetic protein clustering and signaling activation in mammalian cells. *Nat. Methods* **10**, 249–252 (2013).
45. Wendland, B. Epsins: adaptors in endocytosis? *Nat. Rev. Mol. Cell Biol.* **3**, 971–977 (2002).

46. Hawryluk, M. J. *et al.* Epsin 1 is a polyubiquitin-selective clathrin-associated sorting protein. *Traffic* **7**, 262–281 (2006).

47. Chen, H. *et al.* Epsin is an EH-domain-binding protein implicated in clathrin-mediated endocytosis. *Nature* **394**, 793–797 (1998).

48. Aguilar, R. C., Watson, H. A. & Wendland, B. The yeast Epsin Ent1 is recruited to membranes through multiple independent interactions. *J. Biol. Chem.* **278**, 10737–10743 (2003).

49. Dupre, S., Urban-Grimal, D. & Haguenauer-Tsapis, R. Ubiquitin and endocytic internalization in yeast and animal cells. *Biochim. Biophys. Acta BBA-Mol. Cell Res.* **1695**, 89–111 (2004).

50. Taylor, M. J., Perrais, D. & Merrifield, C. J. A high precision survey of the molecular dynamics of mammalian clathrin-mediated endocytosis. *PLoS Biol.* **9**, e1000604 (2011).

51. Kennedy, M. J. *et al.* Rapid blue-light–mediated induction of protein interactions in living cells. *Nat. Methods* **7**, 973–975 (2010).

52. Zeno, W. F. *et al.* Synergy between intrinsically disordered domains and structured proteins amplifies membrane curvature sensing. *Nat. Commun.* **9**, 4152 (2018).

53. Angelova, M. I. & Dimitrov, D. S. Liposome electroformation. *Faraday Discuss. Chem. Soc.* **81**, 303–311 (1986).

54. Aguet, F. *et al.* Membrane dynamics of dividing cells imaged by lattice light-sheet microscopy. *Mol. Biol. Cell* **27**, 3418–3435 (2016).

55. Aguet, F., Antonescu, C. N., Mettlen, M., Schmid, S. L. & Danuser, G. Advances in analysis of low signal-to-noise images link dynamin and AP2 to the functions of an endocytic checkpoint. *Dev. Cell* **26**, 279–291 (2013).